



# Projection Structure of a Plant Vacuole Membrane Aquaporin by Electron Cryo-crystallography

**Mark J. Daniels<sup>1</sup>, Maarten J. Chrispeels<sup>2</sup> and Mark Yeager<sup>1,3\*</sup>**

<sup>1</sup>The Scripps Research Institute,  
Department of Cell Biology  
10550 North Torrey Pines  
Road, La Jolla, CA 92037, USA

<sup>2</sup>University of California  
Department of Biology, 9500  
Gilman Drive, La Jolla, CA  
92093, USA

<sup>3</sup>Division of Cardiovascular  
Diseases, Scripps Clinic  
10660 North Torrey Pines  
Road, La Jolla, CA 92037  
USA

The water channel protein  $\alpha$ -TIP is a member of the major intrinsic protein (MIP) membrane channel family. This aquaporin is found abundantly in vacuolar membranes of cotyledons (seed storage organs) and is synthesized during seed maturation. The water channel activity of  $\alpha$ -TIP can be regulated by phosphorylation, and the protein may function in seed desiccation, cytoplasmic osmoregulation, and/or seed rehydration.  $\alpha$ -TIP was purified from seed meal of the common bean (*Phaseolus vulgaris*) by membrane fractionation, solubilization in diheptanoylphosphocholine and anion-exchange chromatography. Upon detergent removal and reconstitution into lipid bilayers,  $\alpha$ -TIP crystallized as helical tubes. Electron cryo-crystallography of flattened tubes demonstrated that the crystals exhibit plane group *p*2 symmetry and *c*2*2*2 pseudosymmetry. Since the 2D crystals with *p*2 symmetry are derived from helical tubes, we infer that the unit of crystallization on the helical lattice is a dimer of tetramers. A projection density map at a resolution of 7.7 Å revealed that  $\alpha$ -TIP assembles as a 60 Å × 60 Å square tetramer. Each subunit is formed by a heart-shaped ring comprised of density peaks which we interpret as  $\alpha$ -helices. The similarity of this structure to mammalian plasma membrane MIP-family proteins suggests that the molecular design of functionally analogous and genetically homologous aquaporins is maintained between the plant and animal kingdoms.

© 1999 Academic Press

\*Corresponding author

**Keywords:** aquaporin; electron cryo-microscopy; image analysis; projection map; tonoplast intrinsic protein

## Introduction

The plant vacuole is a multifunctional organelle that plays important roles in cellular osmoregulation, metabolism, storage of plant defense chemicals, and plant water relations (Boller & Wiemken, 1986; Matile, 1987; Wink, 1993). The vacuolar membrane (tonoplast) is an essential component for these activities, as it regulates the molecular traffic into and out of the vacuole (Martinolia, 1992). One type of vacuole, the protein storage vacuole (PSV), is present throughout the plant, but especially in the storage tissues of seeds where

they are formed during embryo maturation (Hoh *et al.*, 1995; Paris *et al.*, 1996; Robinson *et al.*, 1995). In embryonic legume cotyledons, each cell forms thousands of PSVs that sequester storage and defense proteins, metabolites, and minerals during seed development (for reviews, see Bewley & Black, 1978; Craig, 1988; Pernollet, 1978). After germination and during growth of the seedling, the storage proteins are hydrolyzed to provide nutrients for the growing plant.

$\alpha$ -TIP (for tonoplast integral protein) is an aquaporin found in the membranes that surround the PSVs in cotyledons of the common bean *Phaseolus vulgaris*. This aquaporin is thought to passively facilitate transmembrane water flow (reviewed by Maurel *et al.*, 1997). The protein accumulates during embryo maturation and disappears rapidly after germination (Johnson *et al.*, 1989; Melroy & Herman, 1991). Whether its primary role is performed during seed development or after germination is unclear. Nevertheless,  $\alpha$ -TIP is thought to have an important and evolutionarily conserved function, since it shares immunogenic epitopes and

Abbreviations used: 2D, two-dimensional; 3D, three-dimensional; DES, *n*-decanoylsucrose; DHPC, 1,2-diheptanoyl-*n*-glycero-3-phosphocholine; DTT, dithiothreitol; LS, *n*-lauroylsarcosine; MIP, major intrinsic protein; PSV, protein storage vacuole; sd, standard deviation; TEA, triethanolamine; TIP, tonoplast intrinsic protein.

E-mail address of the corresponding author:  
[yeager@scripps.edu](mailto:yeager@scripps.edu)

sequence identity with seed membrane proteins in a wide variety of plant species (Höfte *et al.*, 1992; Inoue *et al.*, 1995; Johnson *et al.*, 1989; Oliviuss & Hakman, 1995). Prior to germination,  $\alpha$ -TIP may regulate seed dehydration (Robinson & Hinz, 1997), a hypothesis supported by evidence that the rate of seed desiccation affects *Phaseolus* embryo fitness and survival (Sanhewa & Ellis, 1996a,b). Immediately after germination,  $\alpha$ -TIP may regulate the rehydration of PSVs, osmoregulate the cytoplasm during nutrient export from the PSVs, or adjust vacuolar volume as the central vacuole reforms (reviewed by Maurel *et al.*, 1997).

The major intrinsic protein (MIP) family is highly conserved, with members appearing in plants, animals, fungi, and bacteria (Baker & Saier, 1990). The family progenitor is thought to have arisen from the tandem gene duplication of a putative three transmembrane-spanning domain protein (Reizer *et al.*, 1993). MIP proteins possess six putative hydrophobic transmembrane domains and an Asn-Pro-Ala consensus sequence (often termed the "NPA box"), which is duplicated between the two halves of the protein. Many proteins of the MIP family form channels for small, generally non-ionic solutes. Aquaporins (AQPs) are a subset of these, the term being the functional definition for water-selective transport (Agre *et al.*, 1993).

$\alpha$ -TIP is a member of the MIP family (Johnson *et al.*, 1990) and is a strict aquaporin, being selective for water and impermeable to ions and small non-polar solutes such as glycerol and urea (Maurel *et al.*, 1995, 1997). An important property of  $\alpha$ -TIP is that it is regulated by phosphorylation. After germination,  $\alpha$ -TIP is phosphorylated *in vivo* by a tonoplast-associated CDPK kinase (Johnson & Chrispeels, 1992), which potentiates water transport when assayed in *Xenopus* oocytes (Maurel *et al.*, 1995). Hence, phosphorylation of  $\alpha$ -TIP may be an essential step to regulate the tissue rehydration that occurs during seed germination (Maurel *et al.*, 1997).

Electron cryo-microscopy and image analysis have been used to determine the 2D structure of several MIP family membrane proteins (Table 1) as well as a 3D structure of AQP1 at a resolution of

$\sim 6$  Å in the membrane plane (Cheng *et al.*, 1997; Li *et al.*, 1997; Walz *et al.*, 1997). AQP1 is a constitutively active aquaporin of the erythrocyte plasma membrane that forms a homotetrameric oligomer, with each subunit appearing as an ellipsoidal barrel of  $\alpha$ -helices with an irregular central density ascribed to the two conserved NPA sequences. As a first step in determining the structure of a tonoplast aquaporin, we present here the purification and crystallization of  $\alpha$ -TIP and the determination of its projection structure by electron cryo-microscopy and image analysis.

## Results

### Purification of $\alpha$ -TIP

$\alpha$ -TIP was purified from bean seeds (Figure 1), where it comprises approximately 2% of the total extractable protein in cotyledons (Johnson *et al.*, 1989). From 100 g of dry mass of seed, 4.8 mg of  $\alpha$ -TIP was routinely obtained. Mature, ungerminated seeds were used so that the purified  $\alpha$ -TIP would be at a physiological ground state of phosphorylation (Johnson & Chrispeels, 1992). When obtained from dry seed,  $\alpha$ -TIP eluted as a single broad peak by anion-exchange chromatography (Figure 1(c)).

By SDS-PAGE  $\alpha$ -TIP was found to have an apparent molecular mass of 29.6 kDa (Figure 1(a) and (b)). This size is close to the molecular mass of 27.1 kDa predicted by the cDNA sequence (Johnson *et al.*, 1990), but is different from the previous estimate of 25 kDa based upon gel chromatography (Johnson *et al.*, 1989, 1990). We ascribe this discrepancy to differences in chromatographic methods, since we obtained a molecular mass of 24 kDa following the previously described method (data not shown) (Johnson *et al.*, 1989).

A minor 28.3 kDa isoform was copurified, along with a possible contaminant of 24.5 kDa (Figure 1(a) and (b)); both may be proteolytic fragments of  $\alpha$ -TIP. A similar minor isoform can be seen in previous studies of  $\alpha$ -TIP (Johnson *et al.*, 1989; Mäder & Chrispeels, 1984). Higher molecular mass bands of  $\alpha$ -TIP labeled protein (Figure 1(b)) are likely to be multimers of  $\alpha$ -TIP.

**Table 1.** Summary of aquaporin projection structures

Aquaporin	Molecular mass (kDa)	Source	Homology to bovine AQP0 (%)	Preservation method	Resolution of 2D map (Å)	Crystal symmetry	Monomer dimensions (Å)	Reference
MIP	27	Seep lens	(100) <sup>a</sup>	Freeze-drying	9	p4	24×27	Hasler <i>et al.</i> (1998)
AQP1/CHIP28	28.5	Mammalian red blood cell	43	Vitreous ice, glucose, trehalose	3.5	p42 <sub>12</sub>	26×34	Jap & Li (1995); Mitra <i>et al.</i> (1995); Walz <i>et al.</i> (1995)
AQPic/P25	27.2	Cicadella digestive tract	38	Vitreous ice	24	p4	25×35	Beuron <i>et al.</i> (1995)
AQPZ	23.7	<i>Escherichia coli</i>	39	Vitreous ice	8	p42 <sub>12</sub>	30×31	Ringler <i>et al.</i> (1999)
$\alpha$ -TIP	27.1	<i>Phaseolus</i> bean seed	35	Vitreous ice, glycerol	7.7	p2	27×32	This paper

<sup>a</sup> Assumed homology; gene and protein sequences not reported.

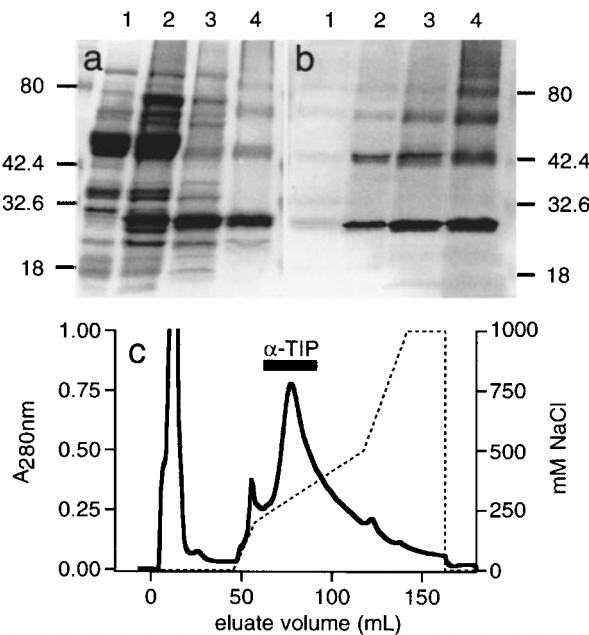


**Figure 1.** The  $\alpha$ -TIP isolation procedure. (a) Coomassie-stained gel. (b) Western immunoblot of equivalent gel, prepared with  $\alpha$ -TIP antiserum. Lane 1, bean homogenate; lane 2, membranes washed with potassium iodide; lane 3, membranes treated with LS; lane 4,  $\alpha$ -TIP peak fraction from anion-exchange chromatography of DHPC-solubilized membranes. Position of molecular mass markers indicated on the sides with the respective molecular mass in kDa. (c) Results of  $\alpha$ -TIP purification by anion-exchange chromatography. The continuous line corresponds to absorbance of eluate at 280 nm. The broken line corresponds to NaCl concentration of elution buffer. The bar indicates collected fraction of  $\alpha$ -TIP.

### Helical crystals of $\alpha$ -TIP

Negatively stained  $\alpha$ -TIP particles appear as  $80 \text{ \AA} \times 80 \text{ \AA}$  particles with a central stain-filled cavity (Figure 2(a)). Their size and shape are similar to the intramembrane particles seen in freeze-fracture micrographs of *P. vulgaris* PSVs (McLean *et al.*, 1994). By *in vitro* reconstitution (Jap *et al.*, 1992; Kühlbrandt, 1992; Yeager *et al.*, 1999), such particles assembled into tubular crystals upon removal of detergent by dialysis (Figure 2(b)). Tubes formed in the presence of several lipids: dimyristoylphosphatidylcholine, soybean phosphatidylcholines, or soybean polar lipids (data not shown). In addition, tubes formed in 0 to 10% glycerol and at lipid to protein molar ratios ranging from 3:1 to 10:1.

Negatively stained, flattened tubes had a constant width of 100 nm and a length of 0.5 to 10  $\mu\text{m}$  (Figure 2(b)). The identity of the crystallized moiety as  $\alpha$ -TIP was confirmed by immunogold labeling using  $\alpha$ -TIP antisera (Figure 2(c)). No labeling was observed using antisera directed against the

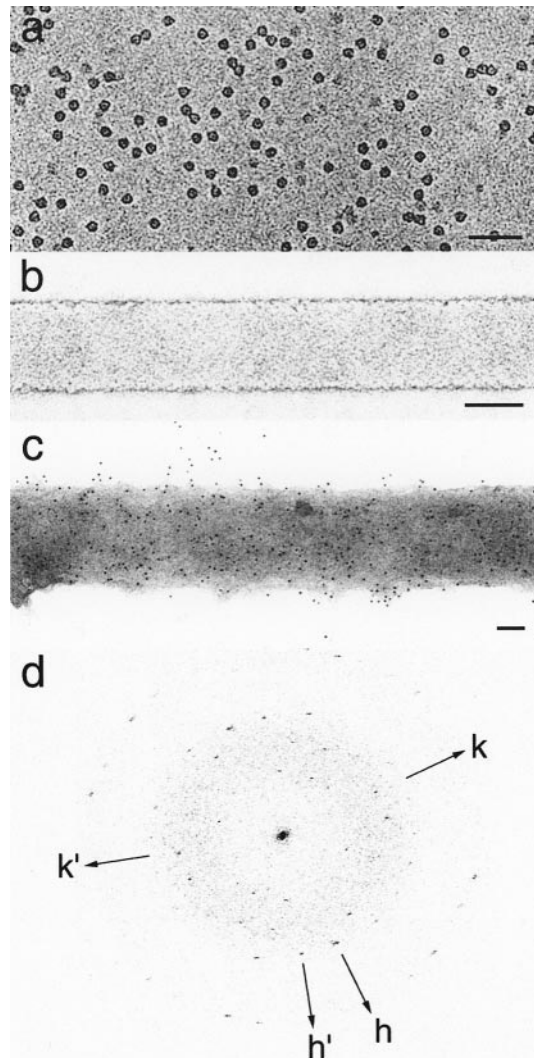


**Figure 2.** Electron micrographs of negatively stained  $\alpha$ -TIP. (a) Individual  $\alpha$ -TIP particles stained with uranyl acetate. (b) Segment of flattened crystal stained with phosphotungstic acid. (c) Segment of flattened crystal immunolabelled with  $\alpha$ -TIP antisera. (d) Computed diffraction pattern from an  $\alpha$ -TIP crystal, showing the axes ( $h$ ,  $k$  and  $h'$ ,  $k'$ ) of the superimposed, nearly rectangular lattices arising from the top and bottom layers of the flattened tube. The scale bar in (a) to (c) represents 50 nm.

related plant tonoplast aquaporin  $\gamma$ -TIP (Höfte *et al.*, 1992) (data not shown).

When imaged by electron cryo-microscopy in vitreous ice over holes in the carbon support (Unwin, 1995), tubes of  $\alpha$ -TIP exhibited layer-line diffraction, demonstrating that they are helical crystals (data not shown). Layer-lines were not observed in diffraction patterns calculated from images recorded using a continuous carbon support, indicating that the tubes had flattened onto the carbon support. In this case, the molecules were arranged as 2D crystals, since optical diffraction patterns typically showed two superimposed,

non-overlapping, nearly rectangular lattices arising from the top and bottom layers of the flattened tube (Figure 2(d)). The 2D crystals were well preserved either in vitreous ice or dried and frozen using glycerol as a cryo-protectant.

### Image analysis of crystals

Flattened tubes were not sufficiently wide to allow recording of electron diffraction patterns; therefore, structure factors were derived by Fourier transformation of the images. The unit cell was nearly rectangular with ( $\pm sd$ ) axes of  $a = 101.2(\pm 0.6)$  Å and  $b = 77.7(\pm 0.7)$  Å and a projected angle of  $90.6(\pm 0.3)^\circ$ . The program MMBOXA was used to fit sinc-functions to the Fourier transform spots by a least-squares method (Amos *et al.*, 1982). A minimal plane group symmetry of  $p2$  was predicted by the program ALLSPACE (Table 2). Analysis of averaged diffraction spot amplitudes in

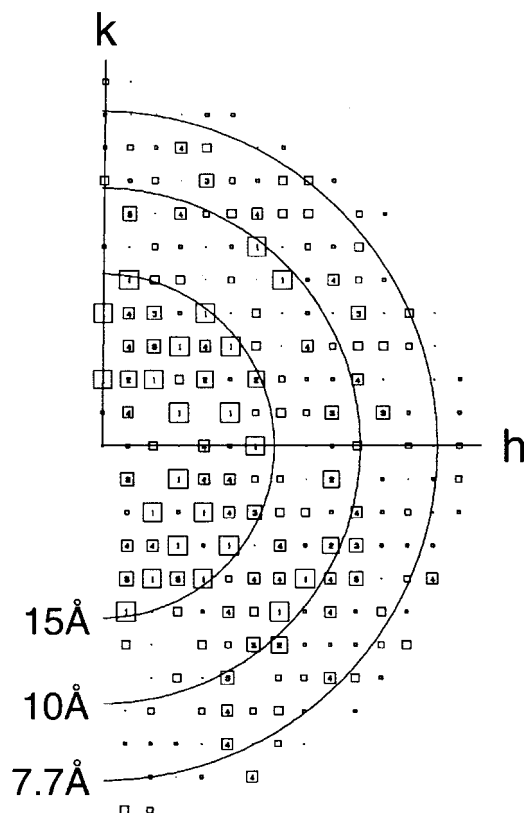


**Figure 3.** Plot of final  $p2$  lattice dataset, showing the combined phase error for each unique reflection. After the merged data were vector averaged, the average phase of each reflection was weighted by its deviation from the theoretical centrosymmetric phase value of  $0^\circ$  or  $180^\circ$ . Increasing phase error is represented as boxes of decreasing size with eight increments:  $1 < 8^\circ$ ,  $2 < 14^\circ$ ,  $3 < 20^\circ$ ,  $4 < 30^\circ$ ,  $5 < 40^\circ$ ,  $6 < 50^\circ$ ,  $7 < 60^\circ$ ,  $8 < 70^\circ$ . Numbers for the first four increments are printed inside the boxes. Above an average phase error of  $90^\circ$ , noise will be greater than signal. Arcs out from the plot origin (0,0) indicate resolution.

narrow resolution bands using MMBOXA showed significant data present to  $7$  Å resolution in most images (data not shown). Images could be sorted into two mirror-image groups according to patterns of diffraction intensity and unit cell angle, indicating good preservation of both sides of the 2D crystals. The  $a$  axis was found to be at an angle of  $\sim 7^\circ$  relative to the longitudinal axis of the tube. Data from 15 images with tilt angles of  $0^\circ$  to  $10^\circ$  were averaged and refined (Table 3).

Systematic weaknesses were seen for  $(h+k)$  odd reflections (Figure 4), suggesting a centered lattice. Concomitantly, analysis of the internal phase residual for reflections with IQ values (Henderson *et al.*, 1986) of 1 to 6 and spatial frequencies of  $\geq 7.7$  Å<sup>-1</sup> predicted  $c222$  plane group symmetry (Table 2). However, there are two key violations of this symmetry. Systematic weaknesses were not evident beyond  $10$  Å resolution (Figure 4), and diffraction patterns did not exhibit  $mm$  symmetry (see Figure 5 for an example). Because these characteristics were consistent for all images, we conclude that the actual symmetry is only  $p2$  and that features suggesting higher symmetry are the result of  $c222$  pseudosymmetry.

Reflection amplitudes decreased evenly with increasing resolution to  $\sim 7.7$  Å (Figure 6(a)). Image-derived amplitudes typically decrease with increasing resolution at a rate greater than that of electron diffraction-derived amplitudes (Baldwin *et al.*, 1988). To correct for this resolution-dependent loss of contrast in crystals of  $\alpha$ -TIP, image amplitudes were compared to electron diffraction amplitudes from the homologous aquaporin AQP1

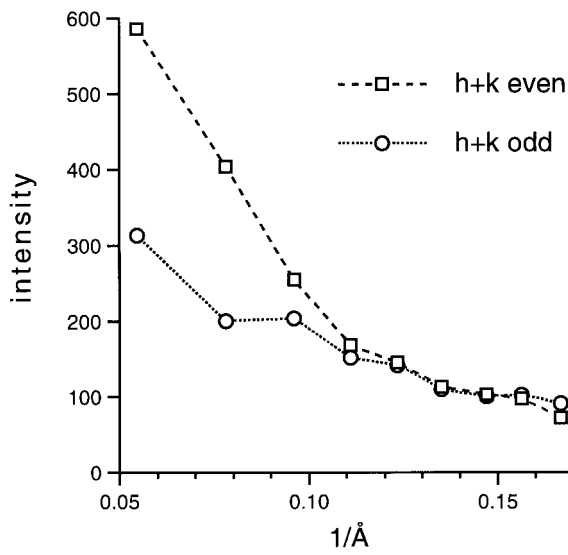


**Figure 4.** Plot comparing amplitude of  $h+k$  even reflections with the amplitude of  $h+k$  odd reflections as a function of resolution. Structure factor amplitudes derived from the final dataset. Data binned and averaged by resolution. Beyond  $10$  Å resolution there is no significant difference between the  $h+k$  even and odd reflections.

**Table 2.** Internal phase residuals of reference image according to plane group

Plane group	Phase residual (deg.) versus other spots <sup>a</sup>	Phase residual (deg.) versus theoretical of 0° or 180° <sup>b</sup>	Target residual (deg.) <sup>c</sup>
<i>p</i> 1	33.4(116)	25.0(116) <sup>d</sup>	-
<i>p</i> 2	37.8(58) <sup>e</sup>	18.9(116)	49.9
<i>p</i> 12_b	23.0(30) <sup>e</sup>	19.9(8)	35.6
<i>p</i> 12_a	26.2(29) <sup>e</sup>	19.9(6)	35.1
<i>p</i> 12_1_b	33.8(30) <sup>e</sup>	21.7(8)	35.6
<i>p</i> 12_1_a	36.8(29)	20.6(6)	35.1
<i>c</i> 12_b	23.0(30) <sup>e</sup>	19.9(8)	35.6
<i>c</i> 12_a	26.2(29)	19.9(6)	35.1
<i>p</i> 222	32.4(117)	19.4(116)	41.6
<i>p</i> 222_1_b	47.1(117)	32.1(116)	41.6
<i>p</i> 222_1_a	47.0(117)	32.1(116)	41.6
<i>p</i> 222_1_2_1	37.1(117) <sup>e</sup>	19.1(116)	41.6
<i>c</i> 222	32.4(117) <sup>e</sup>	19.4(116)	41.6

Number of comparisons shown in parentheses. Internal phase residuals determined using the program ALLSPACE (Valpuesta *et al.*, 1994) for reflections to 7.7 Å resolution with IQ values of 1 to 6. Results shown only for plane groups compatible with the  $\alpha$ -TIP crystal lattice.

<sup>a</sup> Above an average phase error of 90°, noise will be greater than signal.

<sup>b</sup> Above an average phase error of 45°, noise will be greater than signal.

<sup>c</sup> Based on statistics taking Friedel weight into account.

<sup>d</sup> No phase comparisons possible; shown instead are theoretical phase residuals based on the signal-to-noise ratio of the observed amplitudes.

<sup>e</sup> As good as or better than target residual.

(Cheng *et al.*, 1997). At 7.7 Å resolution the estimated image amplitude contrast compared to AQP1 electron diffraction is 56% (Figure 6(b)). This indicated that structure factor amplitudes should be up-weighted by applying a negative temperature factor of  $-150 \text{ \AA}^2$  (Havelka *et al.*, 1995; Unger & Schertler, 1995). The effect will be that amplitudes of reflections at 7.7 Å resolution are increased approximately twofold.

### Projection map of $\alpha$ -TIP

A projection map of  $\alpha$ -TIP calculated at 7.7 Å resolution with *p*2 symmetry (Figure 7) shows that each unit cell is comprised of two roughly square tetramers with an edge length of  $\sim 60 \text{ \AA}$ . Each sub-unit has dimensions of  $27 \text{ \AA} \times 32 \text{ \AA}$  described as a heart-shaped annulus of density peaks with the point at the center of the tetramer. Three to four density peaks form the lobes and cleft, and two

elongated density ridges converge towards the central point.

The presence of *c*222 pseudosymmetry in a single-layer crystal implies the existence of a pseudo-2-fold axis of symmetry within each monomer normal to the plane of the crystal. Such a result correlates with the pseudo-2-fold axis of symmetry seen in monomers of AQP1, which is thought to arise from the tandem repeat of amino acids, and hence repeated structure, in the two halves of MIP-family proteins (Cheng *et al.*, 1997). To examine this possibility, the two halves of the *P. vulgaris*  $\alpha$ -TIP amino acid sequence were compared with each other using the FASTA sequence analysis package (Pearson, 1996). The two best matching segments were 76 amino acid residues in length with an identity of 29% (Figure 8). Comparison scoring of the repeat against a set of globally shuffled sequences showed the inter-half homology of  $\alpha$ -TIP to be two orders of magnitude

**Table 3.** Statistics of the final dataset

Number of images	15		
Cell parameters( $\pm$ sd) (Å; deg)	$a=101.2(\pm 0.6)$ $b=77.7(\pm 0.7)$ ; $\beta=90.6(\pm 0.3)$		
Range of defocus (Å)	-5250 to -12700		
Range of astigmatism (Å)	80 to 1325		
Range of tilt angles (deg.):	0 to 10		
Signal-to-noise ratio of reflections used: $\geq 1.2$ (IQ values 1 to 6)			
Image statistics ( <i>p</i> 2 symmetry; phase angles 0° or 180°)			
Resolution range (Å)	Unique reflections	Phase residual (deg.) <sup>a</sup>	Completeness (%)
$\infty$ -17.4	40	19.3	95
17.3-12.2	42	30.5	95
12.1-10.0	36	32.1	95
9.9-8.6	39	25.4	93
8.5-7.7	41	35.7	91
$\infty$ -7.7	198	28.6	94.3

<sup>a</sup> Phase residual is the difference between the symmetry-constrained phase of 0° or 180° and the observed phase; above a phase residual of 45°, noise will be greater than signal.

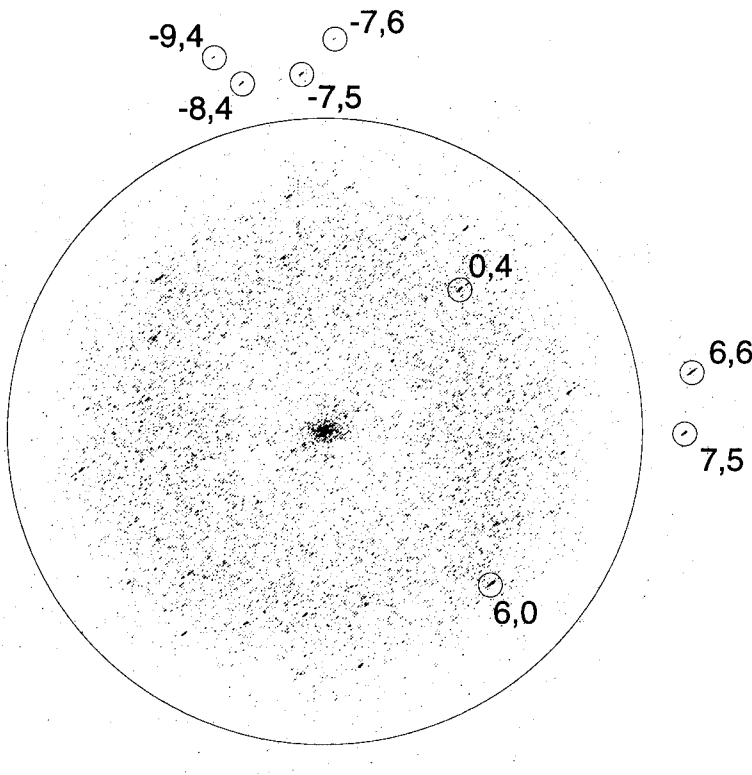


**Figure 5.** Diffraction pattern from image of an uniltted  $\alpha$ -TIP crystal that has been corrected for lattice distortions. Circled reflections shown with lattice indices. Note the lack of  $mm$  symmetry in the diffraction pattern (absence of intensities mirroring the (6, 6) and (-8, 4) reflections). There is breakdown of  $c222$  symmetry as shown by the presence of (-7, 6) and (-9, 4) reflections, which should be absent in a centered lattice, since  $h + k$  is odd for these reflections. Underfocus is approximately -6000 Å, with large circle indicating the first contrast transfer function node.

greater than in AQP0 and four orders of magnitude greater than in AQP1 (Table 4). This result predicts that the in-plane pseudo-2-fold axis of symmetry in monomers of  $\alpha$ -TIP will be more pronounced than in monomers of AQP1.

## Discussion

### Purification of $\alpha$ -TIP

The  $\alpha$ -TIP aquaporin is unique to PSV membranes in seed storage organs and is likely to play an important role in seed maturation and/or seedling development. Its abundance in *Phaseolus* seed membranes facilitated protein purification and crystallization trials. Previous biochemical studies were limited to the characterization of membrane fractions enriched for  $\alpha$ -TIP. Our methods describe the first complete purification of  $\alpha$ -TIP and are amenable to the large-scale isolation of this aquaporin.

Numerous variations of the final protocol were tested. Performing the initial membrane extractions with guanidine hydrochloride efficiently removed contaminating proteins, but also caused  $\alpha$ -TIP to aggregate. The chaotropes urea and sodium iodide were used instead, as milder although less effective alternatives. Treatment of membranes with the mild ionic detergent LS was essential in removing extrinsic membrane proteins prior to membrane solubilization. For solubilizing PSV membranes, the non-ionic detergents *n*-octylglucoside and DHPC were tested. Optimal results were obtained using DHPC, and anion-exchange chromatography was performed to isolate  $\alpha$ -TIP and exchange DHPC for the milder non-ionic detergent DES. The micelle size of this detergent has been estimated at 10 kDa (Makino *et al.*, 1983). Centrifugal filtration of the final isolate using a 100 kDa molecular mass cut-off membrane was therefore used not only to concentrate tetrameric  $\alpha$ -TIP (~118 kDa) but also to remove detergent micelles.

**Table 4.** Significance of internal protein homology

Aquaporin	Overlap (aa)	Identity (%)	Expectation value <sup>a</sup>
AQpcic	58	22.4	4.62
AQP1	74	23.0	1.58
AQPZ	68	25.0	0.976
AQP0	96	26.0	0.0837
$\alpha$ -TIP	76	28.9	0.000172

<sup>a</sup> Expectation value is the number of times the overlapping sequence would occur in 1000 random shuffles of that sequence (Pearson, 1996).

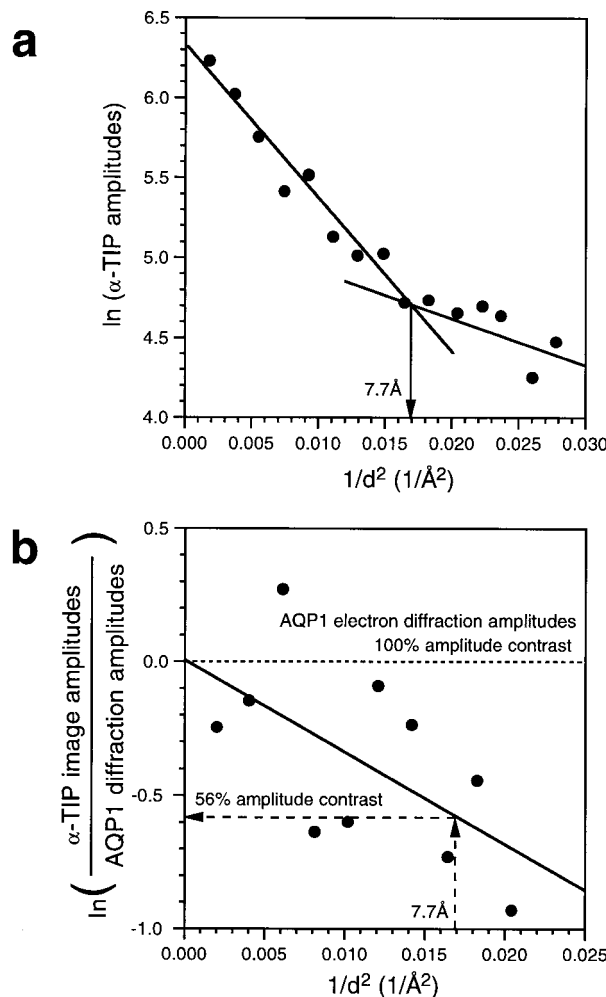


**Figure 6.** Resolution-dependent falloff of  $\alpha$ -TIP image-derived amplitudes. (a) Natural log of  $\alpha$ -TIP image-derived amplitudes plotted against resolution. The linear trend of amplitude falloff breaks down at 7.7 Å. (b) Amplitude contrast shown as the natural log ratio of  $\alpha$ -TIP image amplitudes to AQP1 electron diffraction amplitudes. AQP1 amplitudes (Cheng *et al.*, 1997) were scaled to an amplitude contrast of 100% (0.0) at the origin. Data binned and averaged in resolution bands. Linear fit of data shown, indicating that image-derived amplitudes should be rescaled using a temperature factor of  $-150 \text{ \AA}^2$  to correct for the resolution-dependent loss of contrast (Havelka *et al.*, 1995; Unger & Schertler, 1995). At 7.7 Å resolution the amplitude contrast is 56% ( $-0.58$ ).

Minor proteolytic degradation of the final product was observed (see Figure 1(a) and (b)), similar to previous results (Johnson *et al.*, 1989). AQP1 is glycosylated (van Hoek *et al.*, 1995) and must be deglycosylated for high-resolution structural studies. Since  $\alpha$ -TIP is not glycosylated (Mäder & Chrispeels, 1984), protein purification is simplified and a potential source of structural variability is eliminated.

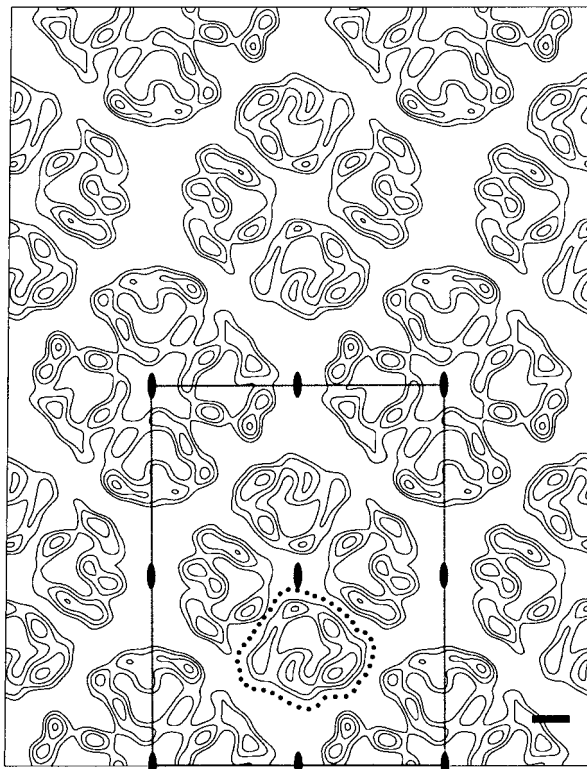


**Figure 7.** Projection map of  $\alpha$ -TIP. Continuous contour lines represent protein density. Unit cell dimensions ( $\pm \text{sd}$ ) are  $a = 101.2(\pm 0.6) \text{ \AA}$ ,  $b = 77.7(\pm 0.7) \text{ \AA}$ , projected angle  $= 90.6(\pm 0.3)^\circ$ . Projection structure of four unit cells determined to 7.7 Å resolution with  $p2$  symmetry applied; monomeric unit within one  $\alpha$ -TIP tetramer is outlined. One unit cell is boxed, with symmetry operators shown. The scale bar represents 10 Å.

### α-TIP aquaporin activity

When expressed in *Xenopus* toad oocytes, the low water channel activity of unphosphorylated  $\alpha$ -TIP is potentiated when  $\alpha$ -TIP is phosphorylated (Maurel *et al.*, 1995). Phosphorylated  $\alpha$ -TIP can be obtained from germinated seed (Johnson & Chrispeels, 1992), or produced enzymatically *in vitro* (Maurel *et al.*, 1995). Since the  $\alpha$ -TIP used for crystallization in this work was isolated from mature, ungerminated seed, we expect that the protein is in a physiological “ground state” of phosphorylation (Johnson & Chrispeels, 1992) and is therefore expected to manifest minimal water channel activity.

### Crystallography of flattened $\alpha$ -TIP tubes

We are encouraged by the good ordering of  $\alpha$ -TIP crystals, which show only a  $\pm 1\%$  variation in unit cell parameters and an amplitude contrast falloff similar to that for crystals of bacteriorhodopsin (Figure 6(b); Schertler *et al.*, 1993). Optical diffraction can be observed beyond 10 Å resolution

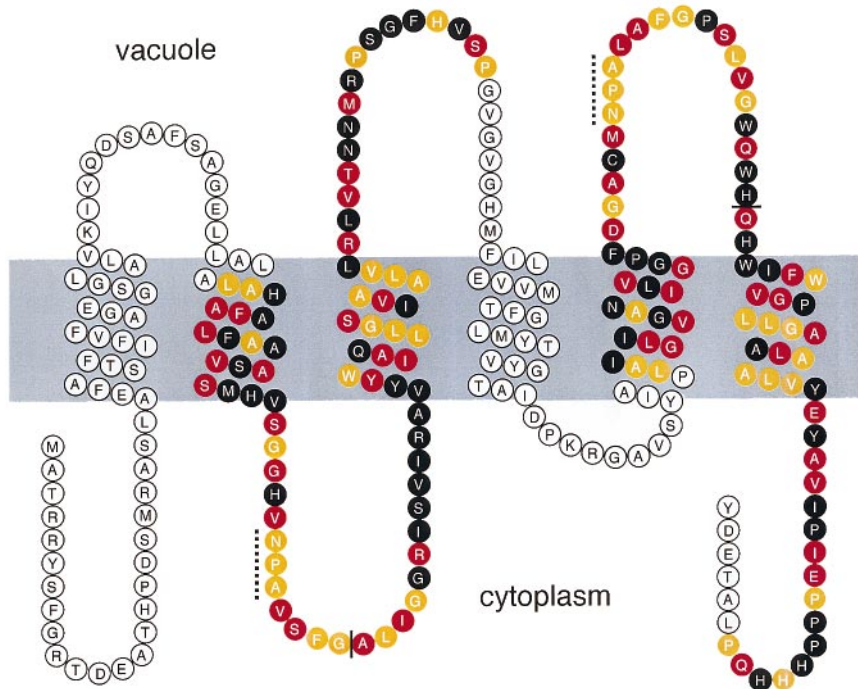


**Figure 8.** Amino acid sequence and internal homology of  $\alpha$ -TIP. Putative membrane topology shown based upon hydrophathy plot analysis (Johnson *et al.*, 1990). Vacuole membrane (tonoplast) represented by gray band. The amino acid N terminus is on the left. Each residue is indicated by the single-letter amino acid code within a circle. The two internal tandem repeats described in Table 4 are shown as a sequence of filled circles. Yellow fill denotes identical residues, red fill denotes similar residues. A filled bar through the sequence indicates gaps in repeated sequence. A broken bar is shown next to the Asn-Pro-Ala MIP-family consensus sequences.

and data extend to  $\sim 7 \text{ \AA}$  resolution. This is somewhat surprising considering that the 100 nm width of the flattened tubes accommodates only 12 to 13 unit cells. The effect of the narrow tube width is a broadening of the diffraction spots and a reduction in the diffraction intensity along the direction parallel with the real space short axis of the tube. Consequently, it was not trivial to precisely define the crystal lattice.

No significant differences were observed between crystals preserved in vitreous ice or crystals dried in glycerol. Polyols such as glycerol, glucose, trehalose, and tannin are commonly used as cryoprotectants and mordants for electron cryocrystallography (Cheong *et al.*, 1996; Külbrandt, 1992; Walz *et al.*, 1997). Glycerol is routinely used in 3D protein crystallization and may contribute to stability and reduce conformational flexibility by replacing water as a solvent and allowing the protein to adopt a more compact conformation (Sousa & Lafer, 1990).

#### p2 plane group symmetry and c222 pseudosymmetry of flattened tubes

Crystallographic 4-fold symmetry as seen in 2D crystals of AQP1 (Mitra *et al.*, 1994; Walz *et al.*, 1994) and MIP (Hasler *et al.*, 1998) is unlikely from structures with helical symmetry. When working with 2D crystals which arise from a flattened helix,

constraints imposed by a helix upon the symmetry must be taken into account. A true helix is formed by repeating motifs that are related to each other by their rotation around and translation along the helical axis (Moody, 1990). A flattened helix retains this pattern but with the rotational increment replaced by a translational one. The resulting two translational increments are the two axes of the observed 2D unit cell. Because the translations occur relative to the helical axis on the helix "surface", unit cells cannot be perpendicular to each other, and consequently only  $p1$  or  $p2$  symmetry is permitted in a flattened helix of an enantiomeric molecule such as  $\alpha$ -TIP (Klug *et al.*, 1958). An additional consideration is that the arrangement of lipids in the curved surface would have to shift during tube flattening, resulting in minor distortions of the crystal packing. Such an effect will become more pronounced with increasing resolution and with decreasing helical diameter, and would be prominent in the narrow tubes of  $\alpha$ -TIP.

Higher symmetry than  $p2$  is suggested by the arrangement of two similar tetramers per unit cell in the projection map of  $\alpha$ -TIP at  $7.7 \text{ \AA}$  resolution (Figure 7). The 2D crystals of the homologous proteins AQP1 and MIP have  $p42_12$  and  $p4$  symmetry, respectively (Table 1). Given the sequence homology and structural similarity of  $\alpha$ -TIP to AQP1 and MIP, planar crystals of  $\alpha$ -TIP would be predicted to show at least  $p4$  plane group symmetry.

The reduced symmetry of  $\alpha$ -TIP crystals may be the result of the protein packing as a dimer of tetramers in order to generate the helical symmetry, or the presence of multiple isoforms causing asymmetry within or between tetramers. Since only  $p1$  or  $p2$  symmetry is permitted on a flattened helix, we infer that the unit of crystallization on the helical lattice is a dimer of tetramers.

The program ALLSPACE predicts  $c222$  symmetry for the flattened tubes of  $\alpha$ -TIP (Table 2). The presence of systematic weaknesses in  $h+k$  odd reflections (Figure 4) also suggests that the crystals belong to the plane group  $c222$ . However, the breakdown of systematic weaknesses at higher resolutions (Figure 5) argues against this plane group. Furthermore, higher resolution reflections do not exhibit  $mm$  symmetry (Figure 5), which forbids rectangular plane groups such as  $c222$ ,  $p22_12_1$ , and  $p22$ .

Our conclusion is that  $\alpha$ -TIP crystals have  $p2$  plane group symmetry and exhibit  $c222$  pseudosymmetry. This pseudosymmetry may be caused by having two tetramers in a unit cell with an angle that is very close to  $90^\circ$  and an internal pseudo-2-fold axis of symmetry within each monomer approximately coincident with the unit cell axes, the result being that the crystal appears to have extra 2-fold axes of symmetry in a centered rectangular lattice. This internal pseudo-2-fold symmetry is likely the result of sequence homology and concomitant structural similarity between the two halves of  $\alpha$ -TIP (Figure 8 and Table 4). True  $c222$  symmetry is impossible because it would imply that the monomer contains a 2-fold axis of symmetry, which is precluded by the non-identity of the N and C-terminal halves of the polypeptide (Figure 8).

### The structure of $\alpha$ -TIP and comparison with other aquaporins

The 2D structure of the plant tonoplast aquaporin water channel  $\alpha$ -TIP presented here at  $7.7\text{ \AA}$  resolution is remarkably similar to erythrocyte aquaporin AQP1 (Jap & Li, 1995; Mitra *et al.*, 1995; Walz *et al.*, 1995) and ovine lens fiber cell MIP (Hasler *et al.*, 1998). Such a result is not unexpected given that these MIP-family proteins share a common ancestor (Reizer *et al.*, 1993) and that the amino acid sequences of  $\alpha$ -TIP and AQP1 are 30% identical. Eight  $\alpha$ -TIP monomers are present in each unit cell and are arranged as a pair of tetramers, identical with crystals of AQP1. Members of the MIP protein family are predicted to have six transmembrane  $\alpha$ -helical domains based on hydrophobicity analysis of the amino acid sequences, as has been shown by the 3D structure of AQP1 (Cheng *et al.*, 1997; Li *et al.*, 1997; Walz *et al.*, 1997).

Since

$\alpha$ -helices pack with a spacing of  $\sim 10\text{ \AA}$ , we interpret the density peaks that form the heart-shaped  $\alpha$ -TIP monomer (Figure 7) as a barrel of six or seven  $\alpha$ -helices. The central protuberance presum-

ably corresponds to loop structures seen in 3D maps of AQP1 (Cheng *et al.*, 1997; Li *et al.*, 1997; Walz *et al.*, 1997). Evidence indicates that the pore-forming motif resides within each subunit rather than in the central cavity of the aquaporin tetramer (Jung *et al.*, 1994), but its location has not as yet been precisely defined. It would be interesting to compare the presented structure of  $\alpha$ -TIP with that of AQP1 for the purpose of distinguishing the C-terminal density due to the additional amino acids of AQP1. This possibility is obviated by both the potential flexibility of the amino termini and possible differences in tilt between monomers of  $\alpha$ -TIP and AQP1.

Although both  $\alpha$ -TIP and AQP1 contain two tetramers per unit cell, the  $\alpha$ -TIP projection unit cell area of  $7900\text{ \AA}^2$  is significantly smaller than the  $10,000\text{ \AA}^2$  area of the AQP1 unit cell. AQP1 is slightly larger than  $\alpha$ -TIP (28.5 kDa *versus* 27.1 kDa), but this does not fully account for the difference. In comparing their projected structures (Figure 9), it can be seen that tetramers of  $\alpha$ -TIP are tightly packed, arranged flush with each other and slightly staggered, whereas tetramers of AQP1 are loosely packed, arranged in line but slightly rotated with respect to each other. These observations suggest that  $\alpha$ -TIP binds fewer lipids. The area occupied by protein in one unit cell is approximately  $5600\text{ \AA}^2$ . Assuming a lipid head-group area of 60 to  $70\text{ \AA}^2$  (Tristram-Nagle *et al.*, 1998), the remaining area would be occupied by 65 to 80 lipid molecules, or eight to ten lipids per monomer. This is significantly less than the 12 to 14 lipids per monomer calculated for crystals of AQP1 (Mitra *et al.*, 1994). The smaller unit cell and tighter packing suggests that  $\alpha$ -TIP crystal contacts are stronger than those of AQP1.

Conservation of structure and function has been indicated between eukaryotic and prokaryotic potassium channels (MacKinnon *et al.*, 1998). Similar conservation of structure between  $\alpha$ -TIP, AQP1 and MIP suggests that the molecular design of functionally analogous and genetically

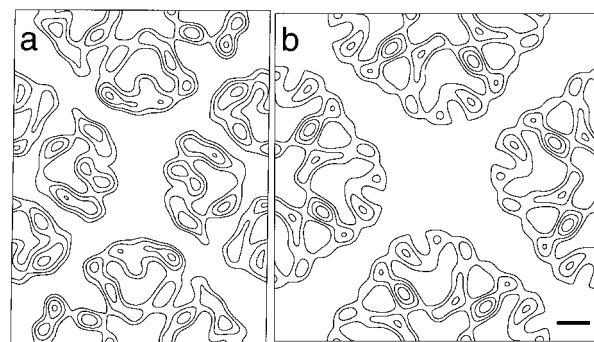


**Figure 9.** Comparison of (a)  $\alpha$ -TIP and (b) AQP1 projection structures at  $7.7\text{ \AA}$  resolution. AQP1 projection structure derived from 3D dataset of electron diffraction results (Cheng *et al.*, 1997). One unit cell shown of each. The scale bar represents  $10\text{ \AA}$ .

homologous aquaporins is maintained between the plant and animal kingdoms.

## Materials and Methods

### Protein purification

PSV membranes were isolated from dry seeds of the common bean (*P. vulgaris* L. cv. Greensleeves) based upon the method of Mäder & Chrispeels (1984). Seed was pulverized with an electric coffee mill (Braun) and resuspended in buffer A (1 M urea, 100 mM triethanolamine (TEA) (pH 7.5), 5 mM EDTA, 5 mM EGTA, 5 mM benzamidine, 4 mM dithiothreitol (DTT) and 2 mM phenylmethylsulfonylfluoride). All procedures were carried out at 4°C unless noted otherwise. Large particles were removed by filtering the homogenate through four layers of cheesecloth, and starch granules were removed by low-speed centrifugation for ten minutes at 100 g. The remaining microsomes were removed from the supernatant by centrifugation for 30 minutes at 25,000 g. The microsomal pellet was resuspended by sonication with a 20 kHz microtip ultrasonic converter at 10% power for ten seconds (model CL4, Heat Systems) in buffer B (1 M potassium iodide, 100 mM TEA (pH 7.5), 10 mM Na<sub>2</sub>S<sub>2</sub>O<sub>3</sub>, 5 mM EDTA, 5 mM EGTA, 5 mM benzamidine and 2 mM DTT), then pelleted as before. Membranes were again resuspended by sonication in buffer C (25 mM TEA (pH 7.5), 1 mM EDTA, 1 mM EGTA, 1 mM DTT) and pelleted as before. Washed microsomes were resuspended by sonication in buffer C, after which *n*-lauroylsarcosine (LS) was added to 0.15% (w/v). The suspension was then stirred for 30 minutes at room temperature. Membranes were collected by ultracentrifugation onto a 50% (w/v) sucrose cushion for 60 minutes at 100,000 g and 12°C. To remove LS, the membranes were resuspended in buffer D (10 mM TEA (pH 7.5), 1 mM DTT, 1 mM EDTA) and then pelleted by ultracentrifugation.

Membranes were solubilized in buffer E (25 mM 1,2-diheptanoyl-*sn*-glycero-3-phosphocholine (DHPC; Avanti Polar Lipids), 40 mM Tris-HCl (pH 8.5), 2 mM DTT) for one hour with stirring at room temperature. Insoluble material was removed by ultracentrifugation at 100,000 g for 30 minutes at 12°C. The supernatant was passed through a 16 mm × 35 mm column of Source 30Q anion-exchange medium (Pharmacia) that had been equilibrated with buffer F (5 mM *n*-decanoylsucrose (DES) in 40 mM Tris-HCl (pH 8.5), 2 mM DTT) at room temperature. Detergent exchange was performed by equilibrating the column with buffer F. Bound protein was eluted with a three-phase linear gradient of 1 M NaCl in buffer F (Figure 1(c)).  $\alpha$ -TIP eluted as a single broad peak at a NaCl concentration of ~300 mM.

Peak fractions were concentrated to ~1 mg/ml in buffer G (5 mM DES, 100 mM NaCl, 40 mM Tris-HCl (pH 8.5), 2 mM DTT) using a Centriplus-100 (Amicon) by centrifugation at 900 g at 12°C. Fractions containing  $\alpha$ -TIP were identified by SDS-PAGE and Western immunoblotting (Sambrook *et al.*, 1989). Chromatographic samples were solubilized in modified SDS-PAGE sample buffer (40 mM Tris-HCl (pH 6.8), 20% (v/v) glycerol, 4% (w/v) SDS, and 100 mM DTT) and incubated at 37°C for 30 minutes. SDS-PAGE chromatography was performed using a 10%-20% linear acrylamide gradient (ReadyGel; Bio-Rad), and immunoblotting was performed with  $\alpha$ -TIP polyclonal antibodies (Johnson *et al.*, 1989). Kaleidoscope (Bio-Rad) prestained protein mol-

ecular mass standards were used. Digitized images of the SDS-PAGE results were corrected for background and contrast using Photoshop (Adobe Systems). Protein concentration was determined using a bicinchoninic acid protein assay (Pierce). Purified  $\alpha$ -TIP was either kept at 4°C or flash-frozen in liquid nitrogen and stored at -80°C in buffer G.

### Two-dimensional crystallization

Helical crystals of  $\alpha$ -TIP were grown by *in vitro* reconstitution (Jap *et al.*, 1992; Kühlbrandt, 1992; Yeager *et al.*, 1999). A solution of  $\alpha$ -TIP (0.5 to 1.5 mg/ml), with soybean phosphatidylcholines (100 µg/ml; Avanti Polar Lipids), decylmaltoside (0.25% (w/v)), 25 mM TEA (pH 7.5), 100 mM NaCl, 3 mM NaN<sub>3</sub>, 1 mM DTT and 0.1 mM butylated hydroxytoluene was preincubated for one to two hours at 25°C. The solution was then placed within the cap of a 0.5 ml polypropylene microcentrifuge tube and sealed with a cellulose dialysis membrane with a molecular mass cutoff of 25,000 Da (Spectra/Por 7, Spectrum, Houston, TX) (Yeager *et al.*, 1999). Dialysis was performed using several 0.5 l changes of 25 mM TEA (pH 7.5), 100 mM NaCl, 3 mM NaN<sub>3</sub>, 1 mM DTT, 0.1 mM butylated hydroxytoluene and 0.1 mM EDTA at 27 to 28°C. For some experiments, 10% (v/v) glycerol was added to the crystallization solution and dialysis buffer. Tubular crystals were harvested after ten to 15 days and were stable for several weeks at 4°C or indefinitely when flash-frozen in liquid nitrogen and stored at -80°C.

### Electron microscopy of negatively stained crystals

Carbon-coated copper grids were prepared by vapor depositing carbon onto copper grids coated with a parlodion film, which was subsequently dissolved in amylose, allowing the carbon to settle onto the grids (Schmutz *et al.*, 1994). The grids were glow-discharged in the presence of amylamine, and then a 5 µl aliquot of crystal-bearing solution was applied to each and incubated for one to two minutes. Grids were blotted to near dryness and stained for 30 to 60 seconds in 1% (w/v) phosphotungstic acid (pH 5.5) or 1% (w/v) uranyl acetate (pH 5), then blotted dry with filter paper (Whatman, no. 2). Immunogold labeling of crystals was performed as described (Zhang & Nicolson, 1989) using  $\alpha$ -TIP polyclonal antibodies (Johnson *et al.*, 1989). The method was modified slightly, with primary and secondary antisera used at a dilution of 1:10 and grids stained with 1% (w/v) uranyl acetate. As a negative control, crystals were immunolabeled with a  $\gamma$ -TIP polyclonal antiserum (Höfte *et al.*, 1992). Low-dose (~10 e<sup>-</sup>/Å<sup>2</sup>) images were recorded on Kodak SO163 film using a Philips CM100 electron microscope operating at an accelerating voltage of 100 kV and a magnification of 52,000 ×.

### Electron cryo-microscopy

Aliquots (5 µl) of crystal-bearing solution containing 10% glycerol were applied for one to two minutes on carbon-coated, rhodium-plated copper grids (Ted Pella, Inc.) that had been glow-discharged in the presence of amylamine. Grids were blotted dry on filter paper, further dehydrated under a gentle stream of dry argon, and frozen by plunging into an ethane slush (-172°C). Specimens without glycerol were preserved in vitreous

ice as described (Mitra *et al.*, 1995). Grids were mounted in a liquid-nitrogen cooled Gatan cryo stage and maintained at  $-184^{\circ}\text{C}$  during electron cryo-microscopy. Low-dose ( $\sim 10 \text{ e}^{-}/\text{\AA}^2$ ) images were recorded on Kodak SO163 film using a Philips CM200 electron microscope equipped with a field-emission gun, operating at an accelerating voltage of 200 kV and a magnification of  $50,000 \times$ .

### Image analysis

Optical diffraction was used to select images with minimal drift that displayed sharp diffraction spots extending to at least  $10 \text{ \AA}$  resolution. Images were digitized in a  $3000 \times 3000$  pixel matrix using a Perkin-Elmer PDS microdensitometer at a step size of  $10 \mu\text{m}$ , corresponding to  $2 \text{ \AA}$  at the level of the specimen.

To calculate image tilt geometry,  $1000 \times 1000$  pixel arrays were digitized using a Zeiss SCAI scanner at a stepsize of  $25 \mu\text{m}$ . Diametrically opposite pairs of arrays were selected on a circular arc spanning  $5^{\circ}$  to  $45^{\circ}$  at the periphery of the exposed area in the micrograph. Defocus values were determined from the contrast transfer function in the Fourier transform of each image. Image pairs with the maximal difference in defocus values defined the axis perpendicular to the tilt axis. The tilt angle and tilt axis were then calculated as described (Amos *et al.*, 1982). Images designated as untilted had less than  $0.6^{\circ}$  tilt.

Diffraction patterns were computed by Fourier transformation of the digitized optical densities. Crystalline areas were boxed, then lattice unbending and contrast transfer function corrections were performed using the MRC suite of programs (Crowther *et al.*, 1996; Henderson *et al.*, 1986, 1990) as described (Yeager *et al.*, 1999). When processing highly boxed crystals, reflections are more accurately determined using MMBOXA, rather than its predecessor MMBOX. MMBOXA was therefore used to extract intensity and phase information from the Fourier transform. CCUNBENDE was used for lattice unbending. Probable plane group symmetry was determined by analysis of symmetry characteristics of the computed Fourier transforms, using phase statistics from the program ALLSPACE (Valpuesta *et al.*, 1994) as a guide (Table 2).

An averaged data set was derived from 12 images from samples dehydrated prior to freezing and three images from samples frozen in vitreous ice (Table 3). ALLSPACE was used to determine the initial  $p2$  phase origin of the reference (best untilted) image, with which the phase origins of the remaining images were refined to  $15 \text{ \AA}$  resolution. Structure factors of reflections with IQ values of 1 through 6 (Henderson *et al.*, 1986) were then merged to  $6 \text{ \AA}$  resolution as described (Mitra *et al.*, 1994) with  $p2$  symmetry constraints applied (Figure 3). Structure factors with a  $z^* \leq 0.005$  were incorporated into the merged data. The program ORIGTILT was used to refine contrast transfer functions and phase origins, initially against the reference image and then against the averaged dataset. Figures of merit were calculated for each reflection and used to weight the averaged amplitude of the reflection (Mitra *et al.*, 1994). To determine the cutoff resolution, the figure of merit weighted average amplitude for each structure factor was determined and plotted against resolution (Figure 6(a)). The resolution cutoff was set to the resolution where the amplitude falloff deviated from a linear correlation. Amplitude falloff with increasing resolution

was compensated by applying a negative temperature factor (Havelka *et al.*, 1995; Unger & Schertler, 1995) determined from the slope of amplitude contrast plotted against resolution (Figure 6(b)). Amplitude contrast was defined as the natural log ratio of  $\alpha$ -TIP image amplitudes to AQP1 electron diffraction amplitudes (Cheng *et al.*, 1997). The 2D projection maps were determined by inverse Fourier transformation of the final dataset with  $p2$  symmetry applied, using software from the CCP4 suite of programs (Collaborative Computational Project, 1994).

### Sequence analysis

Comparision of the two repeated halves of aquaporin amino acid sequence was carried out as described (Reizer *et al.*, 1993), with modifications. Genbank accession numbers for the sequences used were: CAA65799, AQPCIC; U38664, AQPZ; A41616, AQP1; P06624, AQP0; CAA44669,  $\alpha$ -TIP. The program LALIGN (Pearson, 1996) was used to determine regions of internal sequence homology using the BLOSUM50 scoring matrix, with gap and extension penalties of  $-14$  and  $-2$ , respectively. For AQP1, gap and extension penalties of  $-10$  and  $-4$  were used in order to limit sequence homology to either the N-terminal or the C-terminal half of the protein. The statistical significance of the longest repeat was evaluated by the program PRSS (Pearson, 1996), comparing the result of 1000 random sequence shuffles with the repeat sequence.

### Acknowledgments

The authors thank John E. Johnson, Ron Milligan, Rashmi Nunn, Vinzenz Unger and Nigel Unwin for their helpful suggestions and discussions. We thank Anchi Cheng and Rashmi Nunn for their careful reading of the manuscript. The authors are grateful to Anchi Cheng and Alok Mitra for providing AQP1 structure factor data. M.J.D. was supported by a Training Grant in Plant Biology and Macromolecular Structure from the NSF and a NRSA fellowship from the NIH. M.Y. was supported by grants from the NHLBI, the American Heart Association, the Gustavus and Louise Pfeiffer Research Foundation and the Donald E. and Delia B. Baxter Foundation. During this work M.Y. was an Established Investigator of the American Heart Association and Bristol-Myers Squibb and is now a recipient of a Clinical Scientist Award in Translational Research from the Burroughs Wellcome Fund.

### References

- Agre, P., Sasaki, S. & Chrispeels, M. J. (1993). Aquaporins: a family of water channel proteins. *Am. J. Physiol.* **265**, F461.
- Amos, L. A., Henderson, R. & Unwin, P. N. T. (1982). Three-dimensional structure determination by electron microscopy of two-dimensional crystals. *Prog. Biophys. Mol. Biol.* **39**, 183-231.
- Baker, M. E. & Saier, M. H. (1990). A common ancestor for bovine lens fiber major intrinsic protein, soybean nodulin-26 protein, and *E. coli* glycerol facilitator. *Cell*, **60**, 185-186.
- Baldwin, J. M., Henderson, R., Beckman, E. & Zemlin, F. (1988). Images of purple membrane at  $2.8 \text{ \AA}$

- resolution obtained by cryo-electron microscopy. *J. Mol. Biol.* **202**, 585-591.
- Beuron, F., Le Cahérec, F., Guillam, M.-T., Cavalier, A., Garret, A., Tassan, J., Delamarche, C., Schultz, P., Mallouh, V., Rolland, J., Hubert, J., Gouranton, J. & Thomas, D. (1995). Structural analysis of a MIP family protein from the digestive tract of *Cicadella viridis*. *J. Biol. Chem.* **270**, 17414-17422.
- Bewley, J. D. & Black, M. (1978). *Physiology and Biochemistry of Seeds*, Springer-Verlag, Berlin.
- Boller, T. & Wiemken, A. (1986). Dynamics of vacuolar compartmentation. *Annu. Rev. Physiol.* **37**, 137-164.
- Cheng, A., van Hoek, A. N., Yeager, M., Verkman, A. S. & Mitra, A. K. (1997). Three-dimensional organization of a human water channel. *Nature*, **387**, 627-630.
- Cheong, G.-W., Young, H. S., Ogawa, H., Toyoshima, C. & Stokes, D. L. (1996). Lamellar stacking in three-dimensional crystals of  $\text{Ca}^{2+}$ -ATPase from sarcoplasmic reticulum. *Biophys. J.* **70**, 1689-1699.
- Collaborative Computational Project No. 4 (1994). The CCP4 suite: programs for protein crystallography. *Acta Crystallogr. sect. D*, **50**, 760-763.
- Craig, S. (1988). Structural aspects of protein accumulation in developing legume seeds. *Biochem. Physiol. Pflanzen*, **183**, 159-171.
- Crowther, R. A., Henderson, R. & Smith, J. M. (1996). MRC image processing programs. *J. Struct. Biol.* **116**, 9-16.
- Hasler, L., Walz, T., Tittmann, P., Gross, H., Kistler, J. & Engel, A. (1998). Purified lens major intrinsic protein (MIP) forms highly ordered tetragonal two-dimensional arrays by reconstitution. *J. Mol. Biol.* **279**, 855-864.
- Havelka, W. A., Henderson, R. & Oesterhelt, D. (1995). Three-dimensional structure of halorhodopsin at 7 Å resolution. *J. Mol. Biol.* **247**, 726-738.
- Henderson, R., Baldwin, J. M., Downing, K. H., Lepault, J. & Zemlin, F. (1986). Structure of purple membrane from halobacterium halobium: recording, measurement and evaluation of electron micrographs at 3.5 Å resolution. *Ultramicroscopy*, **19**, 147-178.
- Henderson, R., Baldwin, J. M., Ceska, T. A., Zemlin, F., Beckmann, E. & Downing, K. (1990). Model for the structure of bacteriorhodopsin based on high-resolution electron cryo-microscopy. *J. Mol. Biol.* **213**, 899-929.
- Höfte, H., Hubbard, L., Reizer, J., Ludevid, D., Herman, E. M. & Chrispeels, M. J. (1992). Vegetative and seed-specific forms of tonoplast intrinsic protein in the vacuolar membrane of *Arabidopsis thaliana*. *Plant Physiol.* **99**, 561-570.
- Hoh, B., Hinz, G., Jeong, B.-K. & Robinson, D. G. (1995). Protein storage vacuoles form *de novo* during pea cotyledon development. *J. Cell Sci.* **108**, 299-310.
- Inoue, K., Takeuchi, Y., Nishimura, M. & Harashima, I. (1995). Characterization of two integral membrane proteins located in the protein bodies of pumpkin seeds. *Plant Mol. Biol.* **28**, 1089-1101.
- Jap, B. K. & Li, H. (1995). Structure of the osmo-regulated  $\text{H}_2\text{O}$ -channel, AQP-CHIP, in projection at 3.5 Å resolution. *J. Mol. Biol.* **251**, 413-420.
- Jap, B. K., Zulauf, M., Scheybani, T., Hefti, A., Baumeister, W., Aebi, U. & Engel, A. (1992). 2D crystallization: from art to science. *Ultramicroscopy*, **46**, 45-84.
- Johnson, K. D. & Chrispeels, M. J. (1992). Tonoplast-bound protein kinase phosphorylates tonoplast intrinsic protein. *Plant Physiol.* **100**, 1787-1795.
- Johnson, K. D., Herman, E. M. & Chrispeels, M. J. (1989). An abundant, highly conserved tonoplast protein in seeds. *Plant Physiol.* **91**, 1006-1013.
- Johnson, K. D., Höfte, H. & Chrispeels, M. J. (1990). An intrinsic tonoplast protein of protein storage vacuoles in seeds is structurally related to a bacterial solute transporter (GlpF). *Plant Cell*, **2**, 525-532.
- Jung, J. S., Preston, G. M., Smith, B. L., Guggino, W. B. & Agre, P. (1994). Molecular structure of the water channel through aquaporin CHIP. *J. Biol. Chem.* **269**, 14648-14654.
- Klug, A., Crick, F. H. C. & Wyckoff, H. W. (1958). Diffraction by helical structures. *Acta Crystallogr.* **11**, 199-213.
- Kühlbrandt, W. (1992). Two-dimensional crystallization of membrane proteins. *Quart. Rev. Biophys.* **25**, 1-49.
- Li, H., Lee, S. & Jap, B. K. (1997). Molecular design of aquaporin-1 water channel as revealed by electron crystallography. *Nature Struct. Biol.* **4**, 263-265.
- MacKinnon, R., Cohen, S. L., Kuo, A., Lee, A. & Chait, B. T. (1998). Structural conservation in prokaryotic and eukaryotic potassium channels. *Science*, **280**, 106-109.
- Mäder, M. & Chrispeels, M. J. (1984). Synthesis of an integral protein of the protein-body membrane in *Phaseolus vulgaris* cotyledons. *Planta*, **160**, 330-340.
- Makino, S., Ogimoto, S. & Koga, S. (1983). Sucrose monoesters of fatty acids: their properties and interaction with proteins. *Agric. Biol. Chem.* **47**, 319-326.
- Martinoia, E. (1992). Transport processes in vacuoles of higher plants. *Botanica Acta*, **105**, 232-245.
- Matile, P. (1987). The sap of plant cells. *New Phytol.* **105**, 1-26.
- Maurel, C., Kado, R. T., Guern, J. & Chrispeels, M. J. (1995). Phosphorylation regulates the water channel activity of the seed-specific aquaporin α-TIP. *EMBO J.* **14**, 3028-3035.
- Maurel, C., Chrispeels, M., Lurin, C., Tacnet, R., Geelen, D., Riposte, P. & Guern, J. (1997). Function and regulation of seed aquaporins. *J. Exp. Botany*, **48**, 421-430.
- McLean, B., Humphries, J. & Juniper, B. E. (1994). A freeze-fracture study of mesophyll cell membranes in the embryonic *Phaseolus* leaf, in the dry seed and during the initial stages of germination. *Tissue Cell*, **26**, 133-142.
- Melroy, D. L. & Herman, E. M. (1991). TIP, an integral membrane protein of the protein-storage vacuoles of the soybean cotyledon undergoes developmentally regulated membrane accumulation and removal. *Planta*, **184**, 113-122.
- Mitra, A. K., Yeager, M., van Hoek, A. N., Wiener, M. C. & Verkman, A. S. (1994). Projection structure of the CHIP28 water channel in lipid bilayer membranes at 12-Å resolution. *Biochemistry*, **33**, 12735-12740.
- Mitra, A. K., van Hoek, A. N., Wiener, M. C., Verkman, A. S. & Yeager, M. (1995). The CHIP28 water channel visualized in ice by electron crystallography. *Nature Struct. Biol.* **2**, 726-729.
- Moody, M. F. (1990). Image analysis of electron micrographs. In *Biophysical Electron Microscopy* (Hawkes, P. W. & Valdrè, U., eds), pp. 145-288, Academic Press, San Diego, CA.
- Oliviusson, P. & Hakman, I. (1995). A tonoplast intrinsic protein (TIP) is present in seeds, roots, and somatic

- embryos of Norway spruce (*Picea abies*). *Physiol. Plantarum*, **95**, 288-295.
- Paris, N., Stanley, C. M., Jones, R. L. & Rogers, J. C. (1996). Plant cells contain two functionally distinct vacuolar compartments. *Cell*, **85**, 563-572.
- Pearson, W. R. (1996). Effective protein sequence comparison. *Methods Enzymol.* **266**, 227-258.
- Pernollet, J. C. (1978). Protein bodies of seeds: ultrastructure, biochemistry, biosynthesis and degradation. *Phytochemistry*, **17**, 1473-1480.
- Reizer, J., Reizer, A. & Saier, M. H. (1993). The MIP family of integral membrane channel proteins: sequence comparisons, evolutionary relationships, reconstructed pathway of evolution, and proposed functional differentiation of the two repeated halves of the proteins. *Crit. Rev. Biochem. Mol. Biol.* **28**, 235-257.
- Ringler, P., Borgnia, M. J., Stahlberg, H., Maloney, P. C., Agre, P. & Engel, A. (1999). Structure of the water channel AqpZ from *Escherichia coli* revealed by electron crystallography. *J. Mol. Biol.* **291**, 1181-1190.
- Robinson, D. G. & Hinz, G. (1997). Vacuole biogenesis and protein transport to the plant vacuole: a comparison with the yeast vacuole and the mammalian lysosome. *Protoplasma*, **197**, 1-25.
- Robinson, D. G., Hoh, B., Hinz, G. & Jeong, B.-K. (1995). One vacuole or two vacuoles: do protein storage vacuoles arise *de novo* during pea cotyledon development? *J. Plant Physiol.* **145**, 654-664.
- Sambrook, J., Fritsch, E. F. & Maniatis, T. (1989). *Molecular Cloning: A Laboratory Manual*, Cold Spring Harbor Laboratory Press, Cold Spring Harbor, NY.
- Sanhewe, A. J. & Ellis, R. H. (1996a). Seed development and maturation in *Phaseolus vulgaris*. I. Ability to germinate and to tolerate dessication. *J. Exp. Botany*, **47**, 949-958.
- Sanhewe, A. J. & Ellis, R. H. (1996b). Seed development and maturation in *Phaseolus vulgaris*. II. Post-harvest longevity in air-dry storage. *J. Exp. Botany*, **47**, 959-965.
- Schertler, G. F. X., Villa, C. & Henderson, R. (1993). Projection structure of rhodopsin. *Nature*, **362**, 770-772.
- Schmutz, M., Lang, J., Graff, S. & Brisson, A. (1994). Defects of planarity of carbon films supported on electron microscope grids revealed by reflected light microscopy. *J. Struct. Biol.* **112**, 252-258.
- Sousa, R. & Lafer, E. M. (1990). The use of glycerol in crystallization of T7 RNA polymerase: implications for the use of cosolvents in crystallizing flexible proteins. *Methods*, **1**, 50-56.
- Tristram-Nagle, S., Petrache, H. I. & Nagle, J. F. (1998). Structure and interactions of fully hydrated dioleylphosphatidylcholine bilayers. *Biophys. J.* **75**, 917-925.
- Unger, V. M. & Schertler, G. F. X. (1995). Low resolution structure of bovine rhodopsin determined by electron cryo-microscopy. *Biophys. J.* **68**, 1776-1786.
- Unwin, N. (1995). Acetylcholine receptor channel imaged in the open state. *Nature*, **373**, 37-43.
- Valpuesta, J. M., Carrascosa, J. L. & Henderson, R. (1994). Analysis of electron microscope images and electron diffraction patterns of thin crystals of  $\alpha$ 29 connectors in ice. *J. Mol. Biol.* **240**, 281-287.
- van Hoek, A. N., Wiener, M. C., Verbavatz, J.-M., Brown, D., Lipniunas, P. H., Townsend, R. R. & Verkman, A. S. (1995). Purification and structure-function analysis of native, PNGase F-treated, and endo- $\beta$ -galactosidase-treated CHIP28 water channels. *Biochemistry*, **34**, 2212-2219.
- Walz, T., Smith, B. L., Agre, P. & Engel, A. (1994). The three-dimensional structure of human erythrocyte aquaporin CHIP. *EMBO J.* **13**, 2985-2993.
- Walz, T., Typke, D., Smith, B. L., Agre, P. & Engel, A. (1995). Projection map of aquaporin-1 determined by electron crystallography. *Nature Struct. Biol.* **2**, 730-732.
- Walz, T., Hirai, T., Murata, K., Heymann, J. B., Mitsuoka, K., Fujiyoshi, Y., Smith, B. L., Agre, P. & Engel, A. (1997). The three-dimensional structure of aquaporin-1. *Nature*, **387**, 624-627.
- Wink, M. (1993). The plant vacuole: a multifunctional compartment. *J. Exp. Botany*, **44**, 231-246.
- Yeager, M., Unger, V. M. & Nifira, A. K. (1999). Three-dimensional structure of membrane proteins determined by two-dimensional crystallization, electron cryomicroscopy, and image analysis. *Methods Enzymol.* **294**, 135-180.
- Zhang, J.-T. & Nicholson, B. J. (1989). Sequence and tissue distribution of a second protein of hepatic gap junctions, Cx26, as deduced from its cDNA. *J. Cell Biol.* **109**, 3391-3401.

Edited by W. Baumeister

(Received 3 September 1999; accepted 8 October 1999)